

Quantum spin torque driven transmutation of antiferromagnetic Mott insulator

Marko D. Petrović,¹ Priyanka Mondal,¹ Adrian E. Feiguin,² and Branislav K. Nikolić^{1,*}

¹*Department of Physics and Astronomy, University of Delaware, Newark DE 19716, USA*

²*Department of Physics, Northeastern University, Boston, MA 02115, USA*

The standard model of spin-transfer torque (STT) in antiferromagnetic spintronics considers exchange of angular momentum between quantum spins of flowing electrons and noncollinear-to-them localized spins treated as *classical* vectors. These vectors are assumed to realize Néel order in equilibrium, $\uparrow\downarrow \dots \uparrow\downarrow$, and their STT-driven dynamics is described by the Landau-Lifshitz-Gilbert (LLG) equation. However, many experimentally employed materials (such as archetypical NiO) are strongly electron-correlated antiferromagnetic Mott insulators (AFMI) where localized spins form a ground state quite different from the unentangled Néel state $|\uparrow\downarrow \dots \uparrow\downarrow\rangle$. The true ground state is entangled by quantum spin fluctuations, leading to expectation value of all localized spins being *zero*, so that LLG dynamics of classical vectors of fixed length rotating due to STT cannot even be initiated. Instead, a fully quantum treatment of *both* conduction electrons and localized spins is necessary to capture exchange of spin angular momentum between them, denoted as *quantum STT*. We use a recently developed time-dependent density matrix renormalization group approach to quantum STT to predict how injection of a spin-polarized current pulse into a normal metal layer coupled to AFMI overlayer via exchange interaction and possibly small interlayer hopping—which mimics, e.g., topological-insulator/NiO bilayer employed experimentally—will induce nonzero expectation value of AFMI localized spins. This new nonequilibrium phase is a spatially inhomogeneous ferromagnet with zigzag profile of localized spins. The total spin absorbed by AFMI increases with electron-electron repulsion in AFMI, as well as when the two layers do not exchange any charge.

Introduction.—The emergence of antiferromagnetic spintronics [1–4] has elevated antiferromagnetic (AF) insulators (AFIs) and metals into active elements of spintronic devices. They exhibit dynamics of their localized spins at a much higher frequencies, reaching THz [4], when compared to ferromagnetic spintronics. Furthermore, the absence of net magnetization forbids any stray magnetic fields, making them largely insensitive to perturbations by external fields. They also exhibit magnetoresistance effects [5, 6] enabling electric readout of changes in the orientations of their localized spins.

Basic spintronic phenomena like spin-transfer torque (STT) [7–10]—where spin angular momentum is exchanged between flowing conduction electrons and noncollinear-to-them [11] localized AF—and spin pumping [12]—where precessing localized AF spins pump pure spin current in the absence of any bias voltage—have been demonstrated recently using different AF materials. The theoretical description [13–22] of these phenomena invariably assumes that localized magnetic moments on two sublattices of the AF material, \mathbf{M}_i^A and \mathbf{M}_i^B , are *classical* vectors with net zero total magnetization in equilibrium due to assumed Néel classical ground state (GS), $\uparrow\downarrow \dots \uparrow\downarrow$. Out of equilibrium, the dynamics of such classical vectors of *fixed* length is described by the Landau-Lifshitz-Gilbert (LLG) equation [23]. The STT is typically introduced into the LLG equation either as a phenomenological term [17–20], or it is calculated microscopically by using steady-state single-particle quantum transport formalism applied to model [13, 14, 21] or first-principles [15, 16, 22] Hamiltonians of AF materials. Recently STT [24] from time-dependent single-particle quantum transport formalism [25] has been coupled [26]

to the LLG equation, capturing additional quantum effects like electronic spin pumping by moving $\mathbf{M}_i^A(t)$ and $\mathbf{M}_i^B(t)$ and the corresponding enhanced damping on them, but this remains conventional [11] *quantum-for-electrons–classical-for-localized-spins* theory of STT.

However, AFIs employed in spintronics experiments are typically strongly electron-correlated transition metal oxides due to narrow *d* bands. For example, widely used [6–10] NiO shares features of both Mott and charge-transfer insulators [27, 28]. Due to quantum (or zero-point) spin fluctuations [29–31], the AF GS is highly *entangled* [30, 32–34], which results in *zero* expectation value of all localized spins, $\mathbf{S}_i = 0$ ($\mathbf{M}_i \propto \mathbf{S}_i = 0$). Thus, conventional [11] $\text{STT} \propto \mathbf{s}_i \times \mathbf{S}_i = 0$ due to injected nonequilibrium electronic spin density \mathbf{s}_i *cannot* be initiated because $\mathbf{S}_i(t = 0) \equiv 0$. Even if $|\mathbf{S}_i(t = 0)| \neq 0$ is provoked by spin-rotation-symmetry-breaking anisotropies [35] or impurities (see Supplemental Material [36] for illustrations), the LLG equation is inapplicable [38, 39] because the length $|\mathbf{S}_i(t)| < |\mathbf{S}_i^{\text{Néel}}|$ will be changing in time, with smaller value signifying higher entanglement (unobserved quantum systems exhibit unitary evolution toward states of higher entanglement [40]). Thus, both situations *necessitate* to describe localized spins *fully* quantum mechanically where $\mathbf{S}_i(t)$ is calculated only at the end.

The entanglement in the AF GS leading to $\mathbf{S}_i = 0$ can be illustrated using an example [41, 42] of a one-dimensional (1D) AF quantum spin- $\frac{1}{2}$ Heisenberg chain

$$\hat{H}_{\text{AFI}} = J \sum_{i=1}^{N_{\text{AFI}}-1} \hat{\mathbf{S}}_i \cdot \hat{\mathbf{S}}_{i+1}, \quad (1)$$

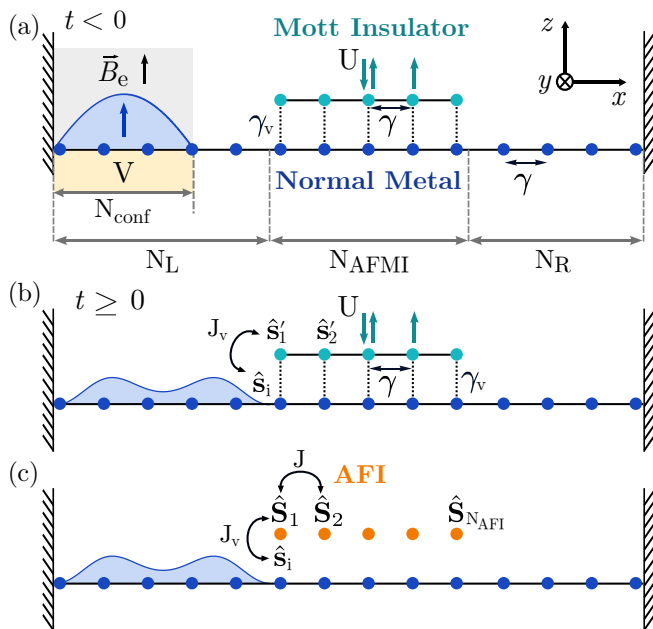


FIG. 1. (a) Schematic view of a “bilayer” [10] for tDMRG calculations where 1D TB chain (blue dots) of $N = N_L + N_{\text{AFMI}} + N_R = 92$ sites, with intrachain hopping γ models the NM surface (such as that of Bi_2Se_3 in experiment of Ref. [10]) through which spin-polarized current pulse is injected. The pulse exerts quantum STT on a Hubbard chain of $N_{\text{AFMI}} = 12$ sites with the on-site Coulomb repulsion U , modeling the surface of strongly electron-correlated AFMI (such as that of NiO in Ref. [7–10]). The electronic spins in two chains interact via interchain exchange interaction J_v , and we consider both $\gamma_v = 0$ and $\gamma_v \neq 0$ interchain hopping where the latter mimics possible hybridization of NM and AFMI via evanescent wavefunctions [22]. For times $t < 0$, $N_e = 12$ noninteracting electrons are confined by potential V within $N_{\text{conf}} = 25$ sites of the L lead (composed of $N_L = 40$ sites), as well as spin-polarized by an external magnetic field \mathbf{B}_e pointing along the z -axis. Concurrently, $N_e^{\text{AFMI}} = 12$ electrons half-fill the AFMI chain. For times $t \geq 0$, V and \mathbf{B}_e are removed, so that electrons propagate as spin-polarized current pulse from the L to the R lead, as illustrated in (b). For comparison, in panel (c) we replace the AFMI from (a) and (b) with AF quantum Heisenberg chain where spin- $\frac{1}{2}$ operators reside on each (orange) site and interact via $J = 4\gamma^2/U$ in Eq. (1) with no charges allowed within this chain.

on N_{AFI} sites. Here $\hat{S}_i^\alpha = \hat{I}_1 \otimes \dots \otimes \frac{1}{2}\hat{\sigma}^\alpha \otimes \dots \otimes \hat{I}_{N_{\text{AFI}}}$ acts nontrivially, as the Pauli matrix $\hat{\sigma}^\alpha$, only on the Hilbert space of site i ; \hat{I}_i is the unit operator; and $J > 0$ is AF exchange interaction. The true GS is easy to write explicitly for small N_{AFI} , such as for $N_{\text{AFI}} = 4$ we find

$$|\text{GS}\rangle = \frac{1}{\sqrt{12}}(2|\uparrow\downarrow\uparrow\downarrow\rangle + 2|\downarrow\uparrow\downarrow\uparrow\rangle - |\uparrow\uparrow\downarrow\downarrow\rangle - |\downarrow\downarrow\uparrow\uparrow\rangle - |\downarrow\downarrow\uparrow\uparrow\rangle - |\uparrow\uparrow\downarrow\downarrow\rangle). \quad (2)$$

Its energy, $\langle \text{GS} | \hat{H}_{\text{AFI}} | \text{GS} \rangle = -2J$, is lower than the energy of the unentangled (i.e., direct-product) Néel state, $\langle \uparrow\downarrow\uparrow\downarrow | \hat{H}_{\text{AFI}} | \uparrow\downarrow\uparrow\downarrow \rangle = -J$. This is in sharp contrast to fer-

romagnets where quantum spin fluctuations are absent, and both classical $\uparrow\uparrow \dots \uparrow\uparrow$ and its unentangled quantum counterpart $|\uparrow\uparrow \dots \uparrow\uparrow\rangle$ are GS of the respective classical and quantum Hamiltonian [such as Eq. (1) with $J < 0$]—it justifies [38, 39] the picture of interacting classical \mathbf{M}_i in spintronics [11] and micromagnetics [23], even as the size of the localized spin is reduced to that of a single electron spin. Conversely, in the case of many-body entangled [30, 32–34] AF GS, the quantum state of each localized spin subsystem *must* be described by the reduced density matrix, $\hat{\rho}_i = \text{Tr}_{\text{other}} |\text{GS}\rangle\langle \text{GS}|$, where partial trace is performed in the Hilbert subspace of all other localized spins $j \neq i$. The expectation value

$$\mathbf{S}_i \equiv \langle \hat{\mathbf{S}}_i \rangle = \text{Tr} [\hat{\rho}_i \hat{\mathbf{S}}_i], \quad (3)$$

is then identically zero vector, $\mathbf{S}_i = 0$, on all sites (see the SM [36]). The GS in the limit $N_{\text{AFI}} \rightarrow \infty$ is computable by Bethe ansatz [42], and its entanglement ensures $\mathbf{S}_i = 0$. The entanglement in the GS of crystalline realization of a two-dimensional (2D) quantum Heisenberg antiferromagnet or antiferromagnetic Mott insulator (AFMI) realized with cold atoms on a square lattice has been detected by neutron scattering [34] or optically [43], respectively, at ultralow temperatures.

In this Letter, we employ the emerging concept of quantum STT [44–47] where *both* conduction electrons and localized spins are treated fully quantum-mechanically to describe the exchange of spin angular momentum between them. This allows us to predict *nonequilibrium phase transition* of AFMI driven by *absorption* of spin angular momentum from spin-polarized current pulse injected into an adjacent normal metal (NM). To model such genuine quantum many-body problem, we evolve in time a nonequilibrium quantum state of NM/AFMI system via very recently developed [46] time-dependent density matrix renormalization group (tDMRG) approach [48–51] to quantum STT.

Our system geometry in Fig. 1 consists of a NM modeled as 1D tight-binding (TB) chain, which is split into the left (L) and the right (R) leads sandwiching a central region. The conduction electron spins in the central region are exchange coupled to an AFMI chain modeled by Hubbard model with the on-site Coulomb repulsion U . The current pulse, carrying electrons initially spin-polarized in the direction perpendicular to the interface (i.e., along the z -axis in Fig. 1), is injected from the L lead into the central region of NM in order to initiate the AFMI dynamics via quantum STT. Our geometry mimics recent experiment [10] on injection of current pulses into metallic surface of topological insulator Bi_2Se_3 , which then exert spin torque on the surface of NiO overlayer covering Bi_2Se_3 , except that in the experiment spin-orbit coupling polarizes injected electrons in the plane of the interface (i.e., along the y -axis in Fig. 1). Nevertheless, since singlet with $\mathbf{s}_i'(t=0) \equiv 0$ on all sites of AFMI is rotationally invariant, the final spin state of

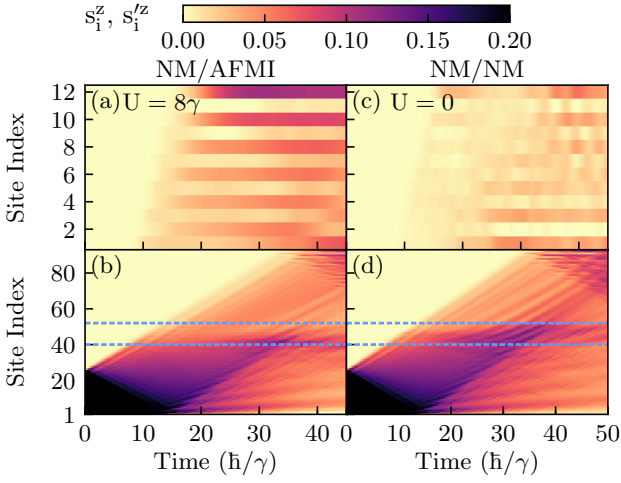


FIG. 2. Spatio-temporal profiles of the z -component of the electronic spin within: (a) AFMI chain with the Coulomb repulsion $U = 8\gamma$; and (c) the same chain with $U = 0$ acting as the second NM chain half-filled with electrons. In both panels $s_i^z(t=0) \equiv 0$, so that only $s_i^z(t) \neq 0$ component is induced by current pulse spin-polarized along the z -axis in Fig. 1(b) and flowing within NM chain whose s_i^z profiles in panels (b) and (d) are driving the profiles in panels (a) and (c), respectively, via quantum STT. The dotted horizontal lines in (b) and (d) mark the boundaries between the leads and the central region of the NM chain in Fig. 1. The interchain exchange is $J_v = 0.5\gamma$ and hopping $\gamma_v = 0$ in Eq. (6).

AFMI driven by quantum STT will be the same for arbitrary spin-polarization of injected electrons.

Our *main* results in Figs. 3–5 demonstrate how quantum STT deposits spin angular momentum [Figs. 4 and 5] into the AFMI by driving its on-site electronic spin expectation value from $s_i^z(t=0) \equiv 0$ in equilibrium toward spatially inhomogeneous profile [Fig. 3] of $s_i^z(t) \neq 0$ [$s_i^x(t) = 0 = s_i^y(t)$], with zigzag pattern $s_{2j-1}^z(t) < s_{2j}^z(t)$ for $j = 1, \dots, N_{\text{AFMI}}/2$. The total spin angular momentum absorbed by AFMI increases with the on-site Coulomb repulsion [Fig. 5(a)], but it is reduced [Figs. 4(c)] when the interchain hopping allows for hybridization of NM and AFMI and electron leakage from AFMI [Fig. 4(a)] into NM [Fig. 4(b)]. Prior to delving into these results, we introduce rigorous notation and useful concepts.

Hamiltonian models and tDMRG method.—The second-quantized many-electron Hamiltonian describing the NM/AFMI system in Fig. 1(a) consists of four terms

$$\hat{H} = \hat{H}_{\text{NM}} + \hat{H}_{\text{AFMI}} + \hat{H}_{\text{NM-AFMI}} + \hat{H}_{\text{V,B}}(t < 0). \quad (4)$$

The first term is 1D TB Hamiltonian of noninteracting electrons within NM chain $\hat{H}_{\text{NM}} = -\gamma \sum_{i=1}^N (\hat{c}_{i\uparrow}^\dagger \hat{c}_{i+1\uparrow} + \hat{c}_{i\downarrow}^\dagger \hat{c}_{i+1\downarrow} + \text{h.c.})$ where $\hat{c}_{i\sigma}^\dagger$ ($\hat{c}_{i\sigma}$) creates (annihilates) an electron with spin $\sigma = \uparrow, \downarrow$ at site i , and γ is the intrachain hopping. These operators act on four possible states at each site i —vacuum $|0\rangle$, spin-up $|\uparrow\rangle$, spin-down $|\downarrow\rangle$, and

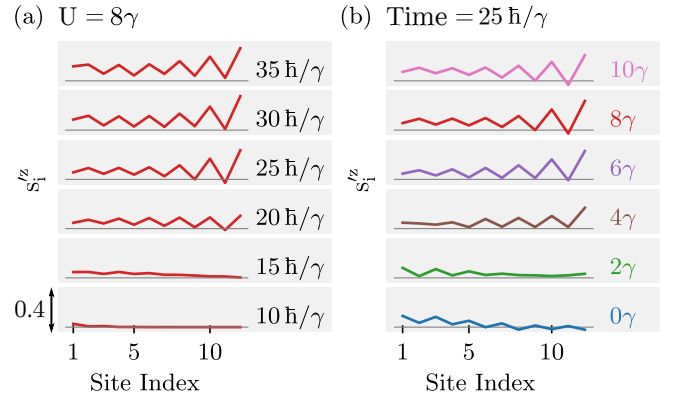


FIG. 3. Spatial profile of the z -component s_i^z of electronic spin within AFMI chain in Fig. 1(b) driven by quantum STT from NM chain: (a) at different times using $U = 8\gamma$ in Eq. (5); and (b) for different U values at time $t = 25\hbar/\gamma$. The interchain exchange is $J_v = 0.5\gamma$ and hopping $\gamma_v = 0$ in Eq. (6).

doubly occupied state $|\uparrow\downarrow\rangle$, so that total Hilbert space of NM/AFMI system has dimension $4^{92} \times 4^{12}$. The interacting electrons within the AFMI chain are described by the Hubbard Hamiltonian [41, 42]

$$\begin{aligned} \hat{H}_{\text{AFMI}} = & -\gamma \sum_{i=1}^{N_{\text{AFMI}}-1} \left(\hat{d}_{i\uparrow}^\dagger \hat{d}_{i+1\uparrow} + \hat{d}_{i\downarrow}^\dagger \hat{d}_{i+1\downarrow} + \text{h.c.} \right) \\ & + U \sum_{i=1}^{N_{\text{AFMI}}} \hat{n}'_{i\uparrow} \hat{n}'_{i\downarrow}. \end{aligned} \quad (5)$$

Here, $\hat{n}'_{i\sigma} = \hat{d}_{i\sigma}^\dagger \hat{d}_{i\sigma}$ are local particle number operators for spin σ at site i of AFMI. The on-site Coulomb repulsion, such as $U = 0$ – 10γ in Fig. 3(b), is expressed in the units of hopping γ (typically $\gamma = 1$ eV) which we use as a unit of energy. The operators for the total number of electrons, $\hat{N}_e^{\text{AFMI}} = \sum_i \hat{n}'_i$, and total electronic spin along the α -axis, $\hat{S}^\alpha = \sum_i \hat{S}_i^\alpha$, are given by sums of local (per-site) charge and spin operators, $\hat{n}'_i = \sum_{\sigma=\{\uparrow,\downarrow\}} \hat{d}_{i\sigma}^\dagger \hat{d}_{i\sigma}$ and $\hat{S}_i^\alpha = \sum_{\sigma=\{\uparrow,\downarrow\}} \hat{d}_{i\sigma}^\dagger \frac{1}{2} \hat{\sigma}_{\sigma\sigma'}^\alpha \hat{d}_{i\sigma'}$, respectively. The interchain exchange interaction J_v between electronic spins within NM and AFMI is described by

$$\begin{aligned} \hat{H}_{\text{NM-AFMI}} = & -J_v \sum_{i=1}^{N_{\text{AFMI}}} \hat{\mathbf{s}}_{i+N_L} \cdot \hat{\mathbf{s}}'_i \\ & - \gamma_v \sum_{i=1}^{N_{\text{AFMI}}} \left(\hat{c}_{i+N_L\uparrow}^\dagger \hat{d}_{i\uparrow} + \hat{c}_{i+N_L\downarrow}^\dagger \hat{d}_{i\downarrow} + \text{h.c.} \right), \end{aligned} \quad (6)$$

where $\hat{\mathbf{s}}_i$ and $\hat{\mathbf{s}}'_i$ are local electron spin operators in NM and AFMI chains, respectively. Here we also add a term with possible $\gamma_v \neq 0$ hopping between N_{AFMI} sites of the central region of the NM chain and N_{AFMI} sites of AFMI in Fig. 1(a), which can arise in realistic devices used in spintronics [7–10] due to evanescent wavefunctions penetrating [22] from the NM surface into the region of AFMI

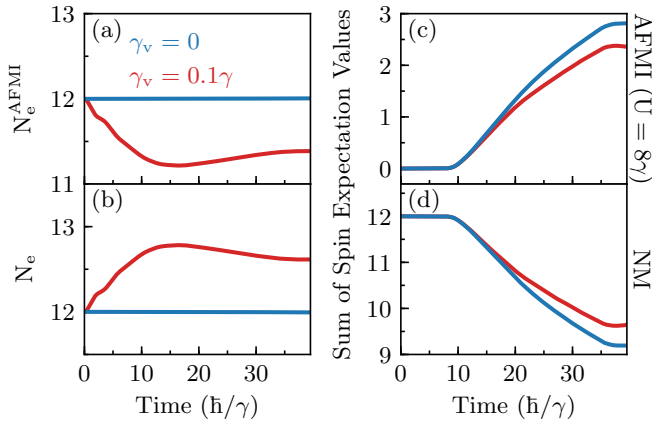


FIG. 4. Time dependence of the total number of electrons within (a) AFMI and (b) NM chains in the setup of Fig. 1(b) for two different interchain hoppings $\gamma_v = 0$ (blue lines) and $\gamma_v = 0.1\gamma$ (red lines). Panels (c) and (d) show the corresponding time dependence of the sum of the z -component of electronic spin expectation values, $\sum_i s_i^z$ and $\sum_i s_i^z$, respectively. The on-site Coulomb repulsion is $U = 8\gamma$ [Eq. (5)] within the AFMI and interchain exchange interaction is $J_v = 0.5\gamma$.

near the interface, thereby leading to charge transfer in equilibrium or current leakage [22] between the two materials. Such normal-metal proximity effect on finite-size Mott insulators can also create exotic many-body states in equilibrium [52]. To prepare the initial state of the conduction electrons in the NM chain, we confine them within N_{conf} sites of the L lead in Fig. 1(a) and polarize their spins along the $+z$ -axis by means of an additional term $\hat{H}_{V,\mathbf{B}}(t < 0) = -V \sum_{i=1}^{N_{\text{conf}}} (\hat{c}_{i\uparrow}^\dagger \hat{c}_{i\uparrow} + \hat{c}_{i\downarrow}^\dagger \hat{c}_{i\downarrow}) - \sum_{i=1}^{N_{\text{conf}}} g\mu_B \hat{s}_i^z B_e^z$. Here $V = 2\gamma$ is the confining potential; B_e^z is the external magnetic field; and $g\mu_B B_e^z = 10\gamma$, where g is the electron gyromagnetic ratio and μ_B is the Bohr magneton. After the initial state is prepared for $t < 0$, $\hat{H}_{V,\mathbf{B}}(t \geq 0)$ is set to zero, so that spin-polarized electrons from the L lead propagate toward the R lead, as illustrated in Fig. 1(b) and computed in Fig. 2.

In the limit $U \gg \gamma$, the half-filled ($n_i = 1$) 1D Hubbard model describes electrons localized one per site, so it can be mapped [41, 42] to isotropic AF quantum spin- $\frac{1}{2}$ Heisenberg chain with the effective Hamiltonian given in Eq. (1). Therefore, for comparison we also analyze the NM/AFI setup in Fig. 1(c) where AFI sites hosts localized spin- $\frac{1}{2}$ operators $\hat{\mathbf{S}}_i$, as described by the Hamiltonian $\hat{H} = \hat{H}_{\text{NM}} + \hat{H}_{\text{AFI}} + \hat{H}_{\text{NM-AFI}} + \hat{H}_{V,\mathbf{B}}(t < 0)$. Here \hat{H}_{NM} is the same as in Eq. (4); \hat{H}_{AFI} is the same as in Eq. (1) where we use $J = 4\gamma^2/U$ as the exchange interaction in the limit $U \gg \gamma$ [41, 42]; the interchain interaction is described by $\hat{H}_{\text{NM-AFI}} = -J_v \sum_{i=1}^{N_{\text{AFI}}} \hat{\mathbf{s}}_{i+N_L} \cdot \hat{\mathbf{S}}_i$ where $J_v = 0.5\gamma$; and $\hat{H}_{V,\mathbf{B}}(t < 0)$ is the same as in Eq. (4).

The tDMRG simulations [48–51] evolve the nonequilibrium state of the whole system in

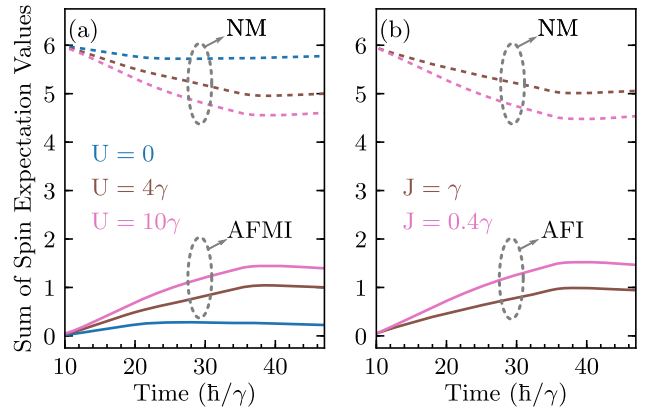


FIG. 5. (a) Time evolution of the sum of electronic spin expectation values within NM chain $\sum_i s_i^z$ (dashed lines) and AFMI chain $\sum_i s_i^z$ (solid lines) in the setup of Fig. 1(b) for different value of the on-site Coulomb repulsion U within the AFMI chain. For comparison, panel (b) plots the same information for the setup in Fig. 1(c) where AFMI is replaced by AF quantum spin- $\frac{1}{2}$ Heisenberg chain with no electrons, so that solid lines are $\sum_i S_i^z$ defined in Eq. (3). For each U in (a), we set the corresponding intrachain exchange interaction J [Eq. (1)] within AFI in (b) as $J = 4\gamma^2/U$.

Fig. 1, $|\Psi(t + \delta t)\rangle = e^{-i\hat{H}\delta t/\hbar}|\Psi(t)\rangle$, using time step $\delta t = 0.1\hbar/\gamma$. We start the propagation with $m = 100$ states and limit the truncation error to 10^{-7} , while the maximal number of states allowed during the evolution is set to $m_{\text{max}} = 400$. Any single-particle expectation value at site i can be obtained from $\hat{\rho}_i(t) = \text{Tr}_{\text{other}} |\Psi(t)\rangle\langle\Psi(t)|$, as exemplified by Eq. (3). Since fermionic leads are not semi-infinite as in usual quantum transport calculations [26], the system in Fig. 1 can be evolved only for a limited time [53–56] before electrons are backscattered by the right boundary which breaks L→R current flow. For example, in Fig. 2 such backscattering occurs at $t \simeq 40\hbar/\gamma$. Nevertheless, the quantum dynamics of the conduction electrons in the NM chain and charge and spin confined within the AFMI chain can be safely assumed to be effectively equivalent to that in an infinite open quantum system before the boundary reflection takes place.

Results and discussion.—The Hubbard 1D chain modeling the AFMI possesses a sizable energy gap Δ_c for charge excitations at $U \gtrsim 2\gamma$, whose value is exactly known [42] in the limit $N_{\text{AFMI}} \rightarrow \infty$ ($\Delta_c = 0.173\gamma$ at $U = 2\gamma$; or $\Delta_c = 0.631\gamma$ at $U = 3\gamma$). In chains of finite length, such as ours with $N_{\text{AFMI}} = 12$ sites, DMRG predicts slightly larger Δ_c values [57]. However, the spin sector of the half-filled Hubbard chain is gapless in the thermodynamic limit. This means that injecting a charge in the AFI is energetically costly, but creating a spin excitation is not. Figures 2(a) and 3 demonstrate that AFMI with $U \gtrsim 4\gamma$ will be driven out of its GS with $s_i^z = 0$ on all sites toward a nonequilibrium phase with

$s_i^z(t) \neq 0$ and $s_i^x = 0 = s_i^y$ due to quantum STT exerted by injected current pulse in the NM chain that is spin-polarized along the z -axis. The spatial profile of $s_i^z(t)$ is inhomogeneous with a zigzag pattern deep in the Mott insulator phase, which distinguishes it from the weak response of the borderline case with $U = 2\gamma$ [Fig. 3(b)] or noninteracting chain with $U = 0$ [Figs. 2(c) and 3(b)].

Even after the current pulse in the NM chain has ended, the spin angular momentum remains deposited within AFMI, with its total value increasing with U [Fig. 5(a)]. Such Mott insulator transmuted into a phase with nonzero total magnetization remains magnetized also when intrachain hopping is switched on, $\gamma_v = 0.1\gamma$, in Fig. 4(c). However, $\gamma_v = 0.1\gamma$ allows electrons to leak from AFMI [Fig. 4(a)] to NM [Fig. 4(b)] chain, so that total spin deposited into AFMI is reduced in Fig. 4(c) when compared to isolated AFMI.

Figure 5 explains, pedagogically and at the microscopic level, quantum STT [44–47] as the transfer of total spin angular momentum from NM conduction electrons (dashed lines in Fig. 5) to confined electrons within the AFMI [solid lines in Fig. 5(a)] or to localized spins within the AFI [solid lines in Fig. 5(b)]. The NM/AFMI case with $U = 10\gamma$ shows that $\sum_i s_i^z(t)$ within AFMI is nearly identical to $\sum_i S_i^z(t)$ within AFI with $J = 4\gamma^2/U$, as anticipated from mapping [41, 42] of AFMI to AFI in the limit $U \gg \gamma$. However, this correspondence fails for $U < 10\gamma$. The absorbed spin by AFMI or AFI can be viewed as multiple excitations of any two-spinon or higher-order spinon states [58], as long as they are compatible with total angular momentum conservation [46].

Conclusions.— In conclusion, we demonstrate how the very recently developed tDMRG [46] approach to *quantum STT* [44–47] makes it possible to study spin torque on strongly electron-correlated antiferromagnets. In contrast, quantum-classical theory of conventional STT [11, 13–22] would conclude that entangled AF true GS does not undergo any current-driven dynamics when its localized spins have zero expectation value at $t = 0$ as the initial state used in this study. Although tDMRG has been previously applied to study charge current through AFMI [53–55] or spin-charge separation [56] in geometries where electrons are injected into AFMI by finite bias voltage, spin-dependent transport phenomena in geometries like Fig. 1 of relevance to spintronics [7–10] remain unexplored. Realistic spintronic devices would require to consider two- or three-dimensional geometries. But Keldysh Green functions [25, 59], as the only available nonequilibrium quantum many-body formalism for higher dimensions and longer times, cannot at present access large U with perturbative self-energies [57, 59], or its nonperturbative implementation can handle [60] only a very few sites. Therefore, this study represents a pivotal test case that provides intuition about quantum STT phenomena in strongly correlated and/or entangled quantum materials, as well as a benchmark [59] for any

future developments via the Keldysh Green functions.

M. D. P., P. M. and B. K. N. were supported by the U.S. National Science Foundation (NSF) Grant No. ECCS 1922689. A. E. F. was supported by the U.S. Department of Energy (DOE) Grant No. DE-SC0019275.

* bnikolic@udel.edu

- [1] V. Baltz, A. Manchon, M. Tsoi, T. Moriyama, T. Ono, and Y. Tserkovnyak, Antiferromagnetic spintronics, *Rev. Mod. Phys.* **90**, 015005 (2018).
- [2] T. Jungwirth, X. Marti, P. Wadley, and J. Wunderlich, Antiferromagnetic spintronics, *Nat. Nanotech.* **11**, 231 (2016).
- [3] J. Železný, P. Wadley, K. Olejník, A. Hoffman, and H. Ohno, Spin transport and spin torque in antiferromagnetic devices, *Nat. Phys.* **14**, 220 (2018).
- [4] B. Jungfleisch, W. Zhang, and A. Hoffmann, Perspectives of antiferromagnetic spintronics, *Phys. Lett. A* **382**, 865 (2018).
- [5] A. Manchon, Spin Hall magnetoresistance in antiferromagnet/normal metal bilayers, *Phys. Status Solidi RRL* **11**, 1600409 (2017).
- [6] L. Baldrati *et al.*, Full angular dependence of the spin Hall and ordinary magnetoresistance in epitaxial antiferromagnetic NiO(001)/Pt thin films, *Phys. Rev. B* **98**, 024422 (2018).
- [7] X.Z. Chen *et al.*, Antidamping-torque-induced switching in biaxial antiferromagnetic insulators, *Phys. Rev. Lett.* **120**, 207204 (2018).
- [8] T. Moriyama, K. Oda, T. Ohkochi, M. Kimata, and T. Ono, Spin torque control of antiferromagnetic moments in NiO, *Sci. Rep.* **8**, 14167 (2018).
- [9] I. Gray *et al.*, Spin Seebeck imaging of spin-torque switching in antiferromagnetic Pt/NiO heterostructures, *Phys. Rev. X* **9**, 041016 (2019).
- [10] Y. Wang *et al.*, Magnetization switching by magnon-mediated spin torque through an antiferromagnetic insulator, *Science* **366**, 1125 (2019).
- [11] D. Ralph and M. Stiles, Spin transfer torques, *J. Magn. Magn. Mater.* **320**, 1190 (2008).
- [12] P. Vaidya, A. Morley, J. van Tol, Y. Liu, R. Cheng, A. Brataas, D. Lederman, E. del Barco, Subterahertz spin pumping from an insulating antiferromagnet, *Science* **368**, 160 (2020).
- [13] A. S. Núñez, R. A. Duine, P. Haney, and A. H. MacDonald, Theory of spin torques and giant magnetoresistance in antiferromagnetic metals, *Phys. Rev. B* **73**, 214426 (2006).
- [14] P. M. Haney and A. H. MacDonald, Current-induced torques due to compensated antiferromagnets, *Phys. Rev. Lett.* **100**, 196801 (2008).
- [15] Y. Xu, S. Wang, and K. Xia, Spin-transfer torques in antiferromagnetic metals from first principles, *Phys. Rev. Lett.* **100**, 226602 (2008).
- [16] M. Stamenova, R. Mohebbi, J. Seyed-Yazdi, I. Rungger, and S. Sanvito, First-principles spin-transfer torque in CuMnAs—GaP—CuMnAs junctions, *Phys. Rev. B* **95**, 060403(R) (2017).
- [17] K. M. D. Hals, Y. Tserkovnyak, and A. Brataas, Phenomenology of current-induced dynamics in antiferro-

- magnets, Phys. Rev. Lett. **106**, 107206 (2011).
- [18] H. V. Gomonay and V. M. Loktev, Spin transfer and current-induced switching in antiferromagnets, Phys. Rev. B **81**, 144427 (2010).
- [19] R. Cheng, J. Xiao, Q. Niu, and A. Brataas, Spin pumping and spin-transfer torques in antiferromagnets, Phys. Rev. Lett. **113**, 057601 (2014).
- [20] R. Cheng, M. W. Daniels, J.-G. Zhu, and D. Xiao, Ultrafast switching of antiferromagnets via spin-transfer torque, Phys. Rev. B **91**, 064423 (2015).
- [21] H. B. M. Saidaoui, A. Manchon, and X. Waintal, Spin transfer torque in antiferromagnetic spin valves: From clean to disordered regimes, Phys. Rev. B **89**, 174430 (2014).
- [22] K. Dolui, M. D. Petrović, K. Zollner, P. Plecháč, J. Fabian, and B. K. Nikolić, Proximity spin-orbit torque on a two-dimensional magnet within van der Waals heterostructure: Current-driven antiferromagnet-to-ferromagnet reversible nonequilibrium phase transition in bilayer CrI₃, Nano Lett. **20**, 2288 (2020).
- [23] R. F. L. Evans, W. J. Fan, P. Chureemart, T. A. Ostler, M. O. A. Ellis, and R. W. Chantrell, Atomistic spin model simulations of magnetic nanomaterials, J. Phys.: Condens. Matter **26**, 103202 (2014).
- [24] A. Suresh, M. D. Petrović, H. Yang, and B. K. Nikolić, Magnon spin-transfer torque from antiferromagnetic insulator to ferromagnetic metal: Time-dependent quantum transport combined with atomistic spin dynamics approach, arXiv:2008.02794 (2020).
- [25] B. Gaury, J. Weston, M. Santin, M. Houzet, C. Groth, and X. Waintal, Numerical simulations of time-resolved quantum electronics, Phys. Rep. **534**, 1 (2014).
- [26] M. D. Petrović, B. S. Popescu, U. Bajpai, P. Plecháč, and B. K. Nikolić, Spin and charge pumping by a steady or pulse-current-driven magnetic domain wall: A self-consistent multiscale time-dependent quantum-classical hybrid approach, Phys. Rev. Applied **10**, 054038 (2018).
- [27] M. Karolak, G. Ulm, T. Wehling, Y. Mazurenko, A. Poteryaev, and A. Lichtenstein, Double counting in LDA+DMFT-The example of NiO, J. Electron Spectrosc. Relat. Phenom. **181**, 11 (2010).
- [28] F. Lechermann, W. Körner, D. F. Urban, and C. Elsässer, Interplay of charge-transfer and Mott-Hubbard physics approached by an efficient combination of self-interaction correction and dynamical mean-field theory, Phys. Rev. B **100**, 115125 (2019).
- [29] A. Singh and Z. Tešanović, Quantum spin fluctuations in an itinerant antiferromagnet, Phys. Rev. B **41**, 11457 (1990).
- [30] S. Humeniuk, Quantum state tomography on a plaquette in the two-dimensional Hubbard model, Phys. Rev. B **100**, 115121 (2019).
- [31] A. Kamra, E. Thingstad, G. Rastelli, R. A. Duine, A. Brataas, W. Belzig, and A. Sudbø, Antiferromagnetic magnons as highly squeezed Fock states underlying quantum correlations, Phys. Rev. B **100**, 174407 (2019).
- [32] T. Roscilde, P. Verrucchi, A. Fubini, S. Haas, and V. Tognetti, Entanglement and factorized ground states in two-dimensional quantum antiferromagnets, Phys. Rev. Lett. **94**, 147208 (2005).
- [33] O. Vafek, N. Regnault, and B. A. Bernevig, Entanglement of exact excited eigenstates of the Hubbard model in arbitrary dimension, SciPost Phys. **3**, 043 (2017).
- [34] N. B. Christensen, H. M. Rønnow, D. F. McMorrow, A. Harrison, T. G. Perring, M. Enderle, R. Coldea, L. P. Regnault, and G. Aeppli, Quantum dynamics and entanglement of spins on a square lattice, PNAS **104**, 15264 (2007).
- [35] E. M. Stoudenmire and S. R. White, Studying two-dimensional systems with the density matrix renormalization group, Annu. Rev. Condens. Matter Phys. **3**, 111 (2011).
- [36] See Supplemental Material at <https://wiki.physics.udel.edu/qttg/Publications>, which includes Ref. [37], for spatial profiles of the expectation value of spin \mathbf{S}_i [Eq. (3)] in 1D and 2D spin- $\frac{1}{2}$ quantum Heisenberg antiferromagnets [Eq. (1)] which possess global spin rotation invariance or they contain a single symmetry-breaking impurity generating magnetic field on one site.
- [37] J. Gray, QUIMB: A Python library for quantum information and many-body calculations, J. Open Source Softw. **3**, 819 (2018).
- [38] R. Wieser, Description of a dissipative quantum spin dynamics with a Landau-Lifshitz-Gilbert like damping and complete derivation of the classical Landau-Lifshitz equation, Euro. Phys. J. B **88**, 77 (2015).
- [39] R. Wieser, Derivation of a time dependent Schrödinger equation as the quantum mechanical Landau-Lifshitz-Bloch equation, J. Phys.: Condens. Matter **28**, 396003 (2016).
- [40] B. Skinner, J. Ruhman, and A. Nahum, Measurement-induced phase transitions in the dynamics of entanglement, Phys. Rev. X **9**, 031009 (2019).
- [41] E. Fradkin, *Field Theories of Condensed Matter Physics* (Cambridge University Press, Cambridge, 2013).
- [42] F. H. Essler, H. Frahm, F. Göhmann, A. Klümper, and V. E. Korepin, *The one-dimensional Hubbard model* (Cambridge University Press, Cambridge, 2005).
- [43] A. Mazurenko, C. S. Chiu, G. Ji, M. F. Parsons, M. Kanász-Nagy, R. Schmidt, F. Grusdt, E. Demler, D. Greif, and M. Greiner, A cold-atom FermiHubbard antiferromagnet, Nature **545**, 462 (2017).
- [44] A. Zhodud, R. Freeman, R. Cao, A. Srivastava, and S. Urazhdin, Spin transfer due to quantum magnetization fluctuations, Phys. Rev. Lett. **119**, 257201 (2017).
- [45] P. Mondal, U. Bajpai, M. D. Petrović, P. Plecháč, and B. K. Nikolić, Quantum spin transfer torque induced nonclassical magnetization dynamics and electron-magnetization entanglement, Phys. Rev. B **99**, 094431 (2019).
- [46] M. D. Petrović, P. Mondal, A. E. Feiguin, P. Plecháč, and B. K. Nikolić, Spintronics meets density matrix renormalization group: Nonclassical magnetization reversal and entanglement growth due to current-pulse-driven quantum spin torque, arXiv:2002.04655 (2020).
- [47] A. Mitrofanov and S. Urazhdin, Energy and momentum conservation in spin transfer, arXiv:2004.01957 (2020).
- [48] A. E. Feiguin, The density matrix renormalization group and its time-dependent variants, in A. Avella and F. Mancini (eds.), AIP Conference Proceedings **1419** (2011).
- [49] S. R. White and A. E. Feiguin, Real-time evolution using the density matrix renormalization group, Phys. Rev. Lett. **93**, 076401 (2004).
- [50] A. J. Daley, C. Kollath, U. Schollwöck, and G. Vidal, Time-dependent density-matrix renormalization-group using adaptive effective Hilbert spaces, J. Stat. Mech. Theor. Exp. P04005 (2004).

- [51] S. Paeckel, T. Köhler, A. Swoboda, S. R. Manmana, U. Schollwöck, and C. Hubig, Time-evolution methods for matrix-product states, *Ann. of Phys.* **411**, 167998 (2019).
- [52] H. Zenia, J. K. Freericks, H. R. Krishnamurthy, and Th. Pruschke, Appearance of “fragile” Fermi liquids in finite-width Mott insulators sandwiched between metallic Leads, *Phys. Rev. Lett.* **103**, 116402 (2009).
- [53] S. K. Irino and K. Ueda, Nonequilibrium current in the one dimensional Hubbard model at half-filling, *J. Phys. Soc. Jpn.* **79**, 093710 (2010).
- [54] F. Heidrich-Meisner, I. González, K. A. Al-Hassanieh, A. E. Feiguin, M. J. Rozenberg, and E. Dagotto, Nonequilibrium electronic transport in a one-dimensional Mott insulator, *Phys. Rev. B* **82**, 205110 (2010).
- [55] L. G. G. V. Dias da Silva, K. A. Al-Hassanieh, A. E. Feiguin, F. A. Reboredo, and E. Dagotto, Real-time dynamics of particle-hole excitations in Mott insulator-metal junctions, *Phys. Rev. B* **81**, 125113 (2010).
- [56] T. Ulbricht and P. Schmitteckert, Is spin-charge separation observable in a transport experiment?, *EPL (Europhysics Letters)* **86**, 57006 (2009).
- [57] J.-P. Joost, N. Schlünzen, S. Hese, M. Bonitz, C. Verdozzi, P. Schmitteckert, and M. Hopjan, Löwdin’s symmetry dilemma within Green functions theory for the one-dimensional Hubbard model, [arXiv:2005.0765](https://arxiv.org/abs/2005.0765) (2020).
- [58] M. Mourigal, M. Enderle, A. Klöpperpieper, J.-S. Caux, A. Stunault, and H. M. Rønnow, Fractional spinon excitations in the quantum Heisenberg antiferromagnetic chain, *Nat. Phys.* **9**, 435 (2013).
- [59] N. Schlünzen, S. Hermanns, M. Scharnke, and M. Bonitz, Ultrafast dynamics of strongly correlated fermions—nonequilibrium Green functions and selfenergy approximations, *J. Phys.: Condens. Matter* **32**, 103001 (2020).
- [60] C. Bertrand, O. Parcollet, A. Maillard, and X. Waintal, Quantum Monte Carlo algorithm for out-of-equilibrium Greens functions at long times, *Phys. Rev. B* **100**, 125129 (2019).